Eur. Phys. J. D **8**, 385–393 (2000)

THE EUROPEAN PHYSICAL JOURNAL D

EDP Sciences

Nuclear quadrupole hyperfine quantum beats in HCl and pyrimidine measured by the pump-probe method using REMPI/LIF detection

H. Lammer, R.T. Carter, and J.R. Huber[a]

Physikalisch-Chemisches Institut der Universität Zürich, Winterthurerstr. 190, 8057 Zürich, Switzerland

Received 26 July 1999 and Received in final form 22 September 1999

Abstract. Coherent time resolved IR-UV double resonance spectroscopy with REMPI and/or LIF detection has been used to measure the nuclear hyperfine structure of a diatomic and a polyatomic molecule. The pump-probe technique was applied and the experimental set up was optimized to achieve highest spectral resolution. Following excitation of the HCl fundamental vibrational transition by a nanosecond IR laser pulse, the nuclear quadrupole coupling constants were determined to be $eQq = -69.51(22)$ MHz for $H^{35}Cl$ and $eQq = -54.40(16)$ MHz for $H^{37}Cl$ in the $J = 1$ and $J = 2$ states of the $v = 1$ level. Nuclear (Cl) spin-rotation interaction was shown to be active with the corresponding coupling constant being $C_I = 0.068(10)$ MHz for $H^{35}Cl$ and $C_I = 0.049(8)$ MHz for $H^{37}Cl$. For pyrimidine a C–H stretch vibration ν_{13} was excited and the quadrupole tensor elements for the rovibronic states $J_{K_a,K_c} = 1_{10}$ and 1_{01} of the $v_{13} = 1$ level were found to be $\chi_{aa} = -3.095(10)$ MHz, $\chi_{bb} = 0.227(10)$ MHz and $\chi_{cc} = 3.322(10)$ MHz. In this case the residual frequency error was reduced to 8 kHz. The results of these jet experiments independently confirm those from millimeter wave and microwave measurements on static gas samples.

PACS. 42.50.Md Optical transient phenomena: quantum beats, photon echo, free-induction decay, dephasings and revivals, optical nutation, and self-induced transparency – 33.15.Pw Fine and hyperfine structure – 33.40.+f Multiple resonances (including double and higher-order resonance processes, such as double nuclear magnetic resonance, electron double resonance, and microwave optical double resonance)

1 Introduction

Over the last two decades, high-resolution coherent time domain spectroscopy has been employed to the measurement of weak effects, either induced by external magnetic or electric fields or originating from intramolecular interactions, in electronically excited states of molecules [1–3]. The time evolution of the coherent excited states can be conveniently measured in a sensitive manner by monitoring their fluorescence emission which exhibits quantum beats superimposed on an exponential decay. After Fourier transformation of this time domain signal, a spectrum in the frequency domain is obtained which has a resolution limited only by the lifetime of the excited states. Importantly the spectrum is essentially free of Doppler broadening.

In applying this spectroscopic method to vibrationally excited molecules in the electronic ground state, an experimental technique is required which not only coherently prepares the states to be investigated but also provides a means to detect their time evolution. Previous work in our group [4,5] and the present study shows that the IR-UV pump probed technique is well-suited to this purpose. Zare and coworkers [6] used a similar setup to demonstrate the time dependence of aligned reagents due the the hyperfine interaction. Here we have demonstrated the feasibility of "quantum beat spectroscopy" for measurements in the electronic ground state by measuring the nuclear hyperfine structure in a diatomic and polyatomic molecule. The excitation and detection scheme employed is shown in Figure 1. Hyperfine levels $|n\rangle$ of a single rotational state in a vibrationally excited level of HCl or pyrimidine (1,3 diazine, $C_4N_2H_4$) were excited coherently $|\Psi\rangle = \sum_n c_n|n\rangle$, with a narrow band infra-red laser pulse. The time evolution of the superposition state $|\Psi(t)\rangle = \sum_n c_n e^{-iE_n t/\hbar}|n\rangle$ was then recorded by monitoring either the undispersed fluorescence from an excited electronic state or the ion signal of the parent mass following a time-delayed UV probe pulse.

The nuclear quadrupole structure in the two molecular systems selected for our experiment has previously been measured using other independent spectroscopic methods. For the diatomic molecule HCl, Kaiser [7] measured the hyperfine structure of the ^{35}Cl isotopomer in the

[a] e-mail: jrhuber@pci.unizh.ch

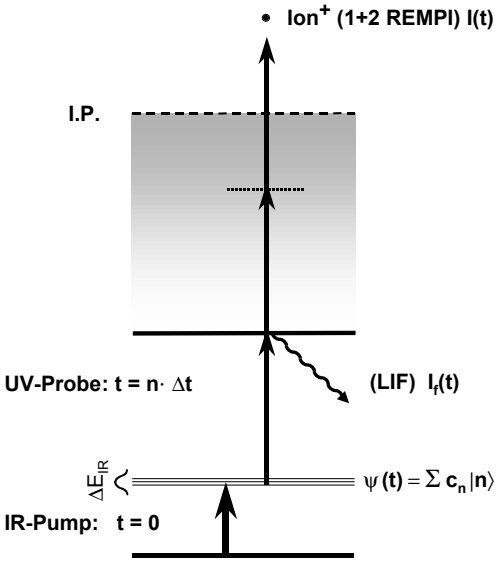

Fig. 1. The principle of the coherent time resolved IR-UV double resonance method used in this work. Following the IR nanosecond pump pulse, the time evolution of the coherent state $\Psi(t)$ is probed by the REMPI and/or LIF method. The UV probe step shown for REMPI detection is that used for pyrimidine $(1+2)$; a $(2+1)$ scheme was used for HCl (see text).

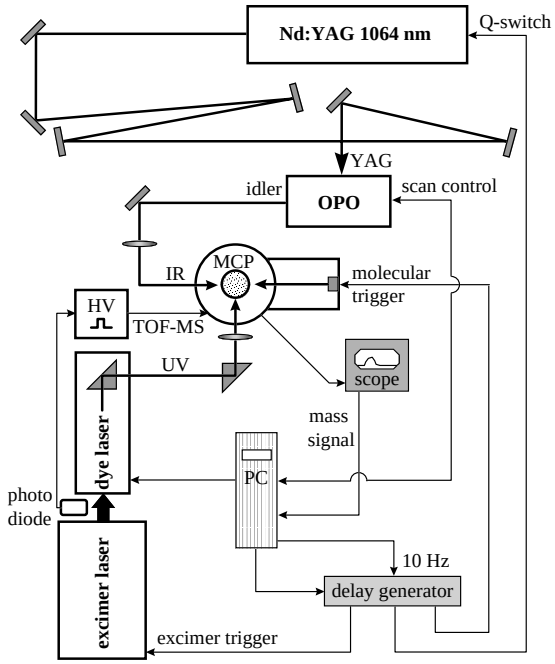

Fig. 2. A schematic of the experimental setup used to record the time resolved IR-UV double resonance measurements (for details see text).

$v = 0, 1, 2$ vibrational levels using a molecular beam electric resonance setup and obtained the pertinent coupling constants. Winnewisser and coworkers [8] used submillimeter wave absorption spectroscopy in conjunction with Lamb dip measurements to study the hyperfine structure of both the ^{35}Cl and ^{37}Cl isotopomers in the $v = 0, 1$ levels. In the case of the polyatomic molecule pyrimidine, Blackman *et al.* [9] used microwave spectroscopy to determine the nuclear hyperfine structure in the vibrational ground state.

2 Experimental

The experimental setup shown in Figure 2 consists of two laser systems which generate the pump and probe pulses and a vacuum chamber equipped with a pulsed molecular beam source and two types of detection system. The IR pump pulse, which has a bandwidth of 0.05 cm^{-1}, was generated by a home-built optical parametric oscillator (OPO) with a $LiNbO_3$ crystal pumped by an injection-seeded Nd:YAG laser at 1064 nm. As a distortion-free TEM_{00} pump beam profile is required for efficient parametric conversion, the pump beam path was extended to 9 m thus reducing the contribution of higher order transversal modes by refraction. The OPO resonator design is similar to that of Minton *et al.* [10] and the cavity optics are resonant for the signal beam (1600 nm). An intra-cavity etalon can be introduced if operation with a bandwidth < 0.5 cm^{-1} is required. The OPO pulse duration is ~ 7 ns. The simultaneously generated idler radiation (~ 3500 nm) was used for the present experiments. Prior to every quantum beat measurement the OPO was tuned to the IR transition of interest by optimizing the cavity length over a range of 2 μm with a piezo-electrically mounted output coupler. As the longitudinal mode spacing of the OPO cavity is 0.025 cm^{-1} and the linewidth of the IR transitions is typically several orders of magnitude smaller, this particular bandwidth ratio allowed pumping of a single rovibronic state with only one longitudinal cavity mode, although the OPO operation itself is not single-mode. The UV-probe pulse was obtained from an excimer pumped tunable dye laser system (Lambda Physik, Scanmate 2E) which has a bandwidth of 0.03 cm^{-1} under etalon operation. It was operated with Coumarin 307 in conjunction with a BBO-frequency doubler or with BMQ dye. The fundamental output energy was 12–15 mJ and the second harmonic generated (SHG) output energy was on the order of 2–3 mJ at a repetition rate of 10 Hz. The duration of the UV pulses was ~ 10 ns. The polarisations of the IR and UV laser pulses were perpendicular to each other.

For the resonance enhanced multiphoton ionisation (REMPI) detection the UV beam passed through a $f = 350$ mm lens, the position of which was manually optimized for a maximum REMPI signal. The ions were extracted by a two-stage ion accelerator of a Wiley-McLaren time of flight mass spectrometer (TOF-MS) system and were detected by a microchannel plate (MCP) detector (Galileo FTD-4000) [11]. The spacing of the accelerator grid electrodes in the TOF-MS is 20 mm and the 1 m drift tube provides a mass-resolution of 120. The repeller and acceleration fields were obtained from a home-built switched high-voltage power supply operating up to 5 kV.

Best space focusing conditions in the mass spectrum were achieved with a constant acceleration field of +2.2 kV/cm and a repeller field of 250 V/cm. In order to ensure zero field conditions and no Stark shifts in the quantum beat experiments, the repeller field was switched on only after 0.3 μs delay with respect to the probe laser and remained on for 10 μs. In all laser induced fluorescence (LIF) experiments the UV laser remained unfocused (about 4 mm diameter) and passed through a baffle arrangement to reduce stray light. The stray light was further attenuated by a 2 mm GG 385 cut off filter (Schott), placed before the photomultiplier tube (PMT) (Hamamatsu, R329-02) and by placing a 300×250 mm matt black aluminium sheet opposite the PMT opening. The output of the PMT was fed through a preamplifier (20 dB, 500 MHz bandwidth). The ion or fluorescence signal was fed to a box car integrator (Stanford SRS 250) and could be monitored on a fast oscilloscope (HP 54510B, 300 MHz, 1 GSa/s). The detection system was triggered by the excimer radiation using a fast photodiode. The experiment was controlled by computer with software developed using LabView.

The anticollinear geometry between IR pump pulse and the molecular beam is illustrated in Figure 3. It allows quantum beats to be recorded over a long observation time with either LIF or REMPI detection. The measurements were performed on a jet-cooled sample obtained by supersonic expansion of the gas mixture (for the HCl experiments: 2% (natural isotopic abundance) in 1.2 bar He; for pyrimidine: 1% in 1.6 bar Ne) through a 0.3 mm nozzle on a piezoelectric valve. This is mounted on the side of the vacuum chamber which is pumped by two turbomolecular pumps backed by membrane pumps. The three other side ports allow the IR and UV beams to enter and the UV beam to leave the chamber. The molecular beam and UV probe beam intersect at right angles in a collision free environment about 120 nozzle diameters downstream from the nozzle. The opening time of the valve was set to 100 μs. The TOF-MS for REMPI detection or the PMT for LIF detection are mounted on top of the vacuum chamber above the intersection point, at mutual right angles to the pump and probe beams.

3 Theoretical aspects

3.1 $H^{35}Cl$ and $H^{37}Cl$

Interaction of the electric field gradients with nuclear electric quadrupole moments couples the molecular rotational angular momentum **J** and nuclear spin **I** to form the total angular momentum $\mathbf{F} = \mathbf{J} + \mathbf{I}$, for $J \geq 1$ and $I \geq 1$. This effect splits a single rotational level into several hyperfine states, described by their total angular momentum quantum number F. In the diatomic case the Hamiltonian for the nuclear quadrupole interaction can be written as [12]

$$H_{\mathrm{Q}} = \frac{1}{2}\frac{eQq_{ZZ}}{I(2I-1)J(2J-1)}[3(\mathbf{I}\cdot\mathbf{J})^2 + \frac{3}{2}(\mathbf{I}\cdot\mathbf{J}) - \mathbf{I}^2\mathbf{J}^2]. \quad (1)$$

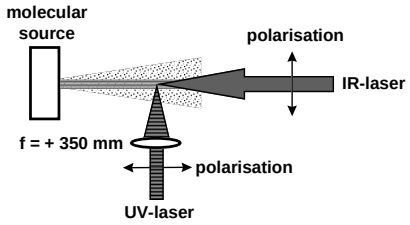

Fig. 3. An illustration of the anticollinear excitation geometry. The IR pump beam is aligned coaxially with the molecular beam. The UV probe laser crosses the sample beam perpendicularly. The detector is above the intersection point at mutual right angles to the IR and UV beams.

Here Q is the quadrupole moment of the nucleus, e is the electron charge and the quantity q_{ZZ} is the value of the molecular field gradient referenced to the lab frame Z direction evaluated for the state $|JM\rangle = |JJ\rangle$ and defined by $q_{ZZ} = \langle JJ|V_{ZZ}|JJ\rangle$. As the field gradients are invariant in the molecule fixed frame, it is convenient to express q_{ZZ} in terms of the principal inertial axis system. For a linear molecule this transformation is given by [13] $q_{ZZ} = -qJ/(2J+3)$. The diagonal matrix elements of H_{Q} in the basis $|JIF\rangle$ are [13]

$$\langle JIF|H_{\mathrm{Q}}|JIF\rangle = \frac{-eqQ}{2}\left[\frac{\frac{3}{4}C(C+1) - I(I+1)J(J+1)}{I(2I-1)(2J-1)(2J+3)}\right], \quad (2)$$

where $C = F(F+1) - I(I+1) - J(J+1)$. Both the isotopes ^{35}Cl and ^{37}Cl have $I = 3/2$ and an energy scheme of the hyperfine levels for both HCl isotopomers is given for the $J = 1$ and $J = 2$ rotational states in Figure 4 (top).

In addition to the nuclear quadrupole interactions, other hyperfine effects might also be active. These include the Cl and H nuclear spin-rotation interactions and the spin-spin interaction between the H and Cl nuclei. Our measurements do indeed reveal the presence of the Cl nuclear spin-rotation interaction (see below), while the other two processes proved too weak to be detected. The nuclear spin-rotation is a magnetic hyperfine effect, which arises from admixture of excited electronic states with the closed shell ground state, and the Hamiltonian for a diatomic molecule is given by $H_{\mathrm{nsr}} = C_{\mathrm{I}}\mathbf{I}\cdot\mathbf{J}$. We note that C_{I}, the associated nuclear magnetic coupling parameter, is approximately proportional to the rotational constant B. The diagonal matrix elements for this interaction are [14]

$$\langle JIF|H_{\mathrm{nsr}}|JIF\rangle = C_{\mathrm{I}}(-1)^{I+J+F+1}\left\{\begin{array}{ccc} F & J & I \\ 1 & I & J \end{array}\right\} \times \sqrt{J(J+1)(2J+1)I(I+1)(2I+1)}. \quad (3)$$

3.2 Pyrimidine

In pyrimidine the two nitrogen nuclei with $I_1 = I_2 = 1$ show identical coupling with J due to symmetry (see insert in Fig. 4). It is convenient [15,16] to describe this

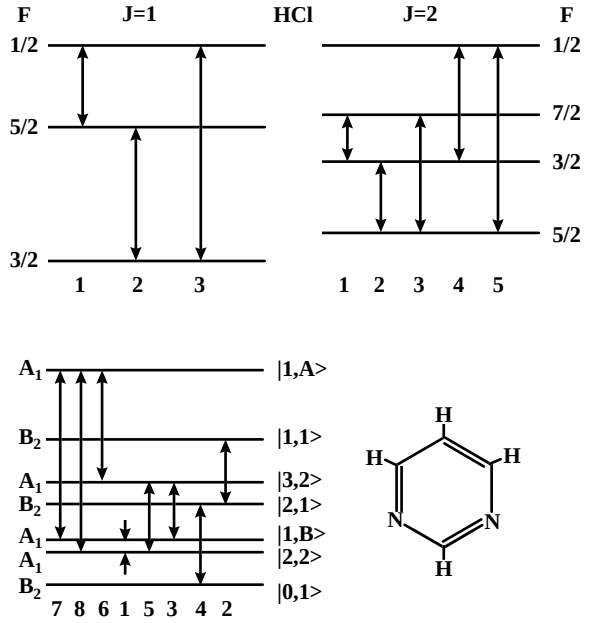

Fig. 4. Nuclear quadrupole splittings for the $J = 1$ and $J = 2$ rotational levels of HCl (top) and for the 1_{01} level in pyrimidine (bottom). The arrows indicate the excited coherences. The hyperfine states in pyrimidine are labelled $|F, I\rangle$, where $|1, A\rangle$ and $|1, B\rangle$ are the eigenstates resulting from mixing of $|1, 2\rangle$ and $|1, 0\rangle$.

particular case of electric quadrupole interaction in the $|JI_1I_2IF\rangle$ basis with the coupling scheme $\mathbf{I} = \mathbf{I}_1 + \mathbf{I}_2$ and $\mathbf{F} = \mathbf{J} + \mathbf{I}$. The general Hamiltonian for the coupling of two nuclear spins I_1 and I_2 in first-order interaction is given by

$$H_{\mathrm{Q}} = H_{\mathrm{Q}}^1 + H_{\mathrm{Q}}^2, \tag{4}$$

where H_{Q}^1 and H_{Q}^2 have the form shown in equation (1). The matrix elements for the Hamiltonian H_{Q} are dependent on a parameter $\chi^+ = eQ_1q_{1ZZ} = eQ_2q_{2ZZ}$ and are given elsewhere [9]. In this coupling scheme, the total nuclear spin quantum number I ranges from 0 to 2 and consequently a rovibrational level is split into nine hyperfine components if $J > 1$ or seven components if $J = 1$ as shown in Figure 4. States with $I = 1$ have B_2 symmetry and have a statistical weight of 1 due to the two equivalent protons, whereas the states with $I = 0$ and $I = 2$ possess A_1 symmetry and have weight 3. As they have the same symmetry, mixing of the $|I, M_I\rangle = |2, 0\rangle$ and $|0, 0\rangle$ states has to be taken into account. Figure 4 (bottom) corresponds to the qualitative hyperfine energy scheme for pyrimidine in the $J_{K_aK_c} = 1_{01}$ rotational level, where the hyperfine states are labeled $|F, I\rangle$. The eigenstates $|1, A\rangle$ and $|1, B\rangle$ respectively result from the mixing as discussed above. The structure for the 1_{10} level is similar, but with hyperfine energies ∼7% larger and of opposite sign.

The time evolution of the pyrimidine quantum beat data was simulated using a density matrix method [17]. The geometry and polarizations of the pump and probe beams were treated following Corney [18]. The vibrationally excited state matrix is given by

$$\rho_{F_m,M_{F_m},F'_m,M'_{F_m}}(0) = \sum_{F_i,M_{F_i}} \langle I_m J_m F_m M_{F_m}|\mu|I_i J_i F_i M_{F_i}\rangle \times \langle I_i J_i F_i M_{F_i}|\mu^*|I'_m J_m F'_m M'_{F'_m}\rangle, \tag{5}$$

and the time evolution is given by $\rho_{F_m,M_{F_m},F'_m,M'_{F_m}}(t) = \rho_{F_m,M_{F_m},F'_m,M'_{F_m}}(0)\exp[\mathrm{i}(\omega_{F_m} - \omega_{F'_m})t]$, where $\omega_{F_m} = E_{F_m}/\hbar$ represents the hyperfine energy. Due to the long lifetime of the vibrationally excited levels, a damping factor can be neglected. The above matrix elements were expressed in terms of the reduced matrix element $|\langle J_m, K_m\|\mu\|J_i, K_i\rangle|^2$ using standard techniques [13], with the mixing of the $|I, M_I\rangle = |2, 0\rangle$ and $|0, 0\rangle$ states also being taken into account. The hyperfine quantum beat signal at time t is given by $\mathrm{Tr}[\rho(t)D]$ where D is the detection matrix [17], which is set up in an analogous manner and assumes a form similar to $\rho(0)$.

4 Results

4.1 $H^{35}Cl$ and $H^{37}Cl$

Applying our IR-UV double resonance method, the IR excitation pulse (τ = 5 ns) was tuned to the R branch of the HCl vibrational fundamental (for $H^{35}Cl$: R(0), R(1): 2906.248 and 2925.898 cm^{-1}; for $H^{37}Cl$: R(0), R(1): 2904.110 and 2923.731 cm^{-1} [19]) to prepare the coherent superposition of hyperfine states (see Fig. 1) in the $J = 0$ or $J = 1$ rotational states of the $v = 1$ level respectively. The superposition state was subsequently probed by a (2+1) REMPI process involving a two-photon resonant step with the $v = 0$ level of the $F^1\Delta_2$ state [20], followed by the ionisation step using a laser wavelength of about 250 nm.

The time evolution of the coherences manifested as quantum beats and shown in Figures 5 and 6, was measured over a delay time range of 0 to 1.2 μs using steps of 12.5 ns which corresponds to a detection bandwidth of 40 MHz. In order to minimise the effect of time dependent laser frequency drift, each data point was averaged over 20 laser shots and the entire range was scanned 20 times. The mass signal of each isotope was clearly resolved in the recorded TOF spectrum with the maximum of the two signals being separated by Δt = 200 ns. The time evolutions of both isotopomers excited into $v = 1$, $J = 1$ and $J = 2$ levels are shown in Figures 5 and 6. In the case of the $J = 1$ results the time evolutions (Fig. 5) exhibit contributions of two strong beating frequencies, where the frequencies for the $H^{35}Cl$ and $H^{37}Cl$ isotopomers differ. For the $J = 2$ results shown in Figure 6, the time evolutions are more complex and the modulation depth is less pronounced than that for $J = 1$, a fact which is to be expected [21]. The difference in the modulation depths for $H^{35}Cl$ and $H^{37}Cl$ is however due to experimental factors such as laser energy and beam alignment.

The Fourier transform of the time evolutions (Figs. 7 and 8) reveals the coherences shown in Figure 4. This was

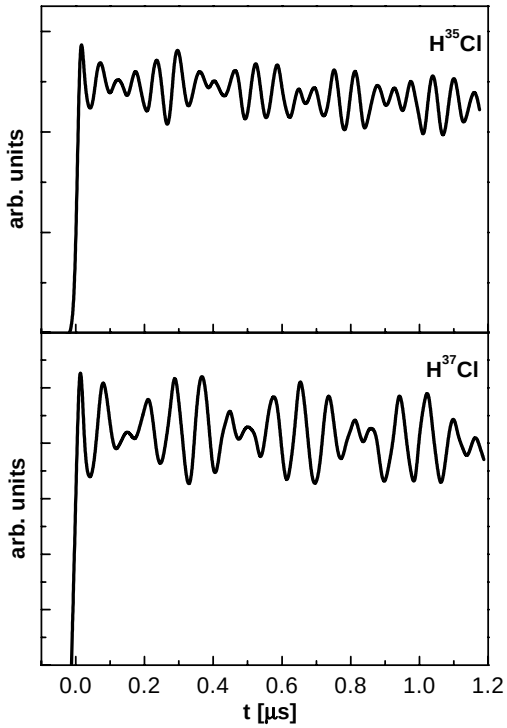

Fig. 5. Time evolutions recorded for the $J = 1$ rotational states of $H^{35}Cl$ and $H^{37}Cl$ exhibiting hyperfine quantum beats.

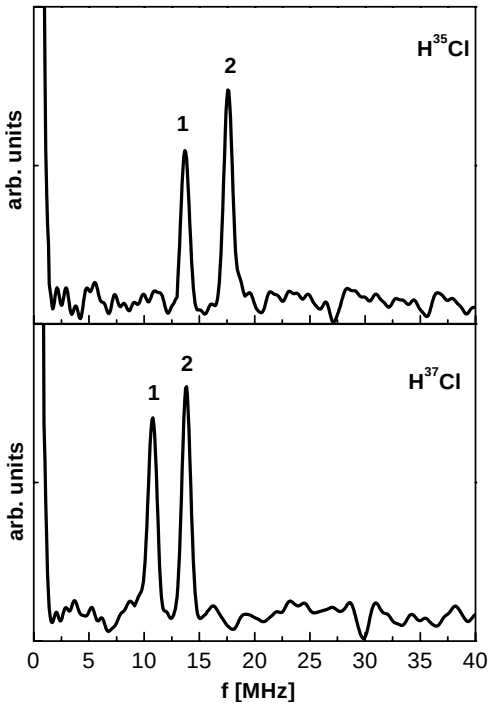

Fig. 7. Frequency domain spectra for the $J = 1$ rotational level in HCl obtained from the real part of the Fourier transform for the time evolutions shown in Figure 5. The labels refer to the coherences detailed in Figure 4.

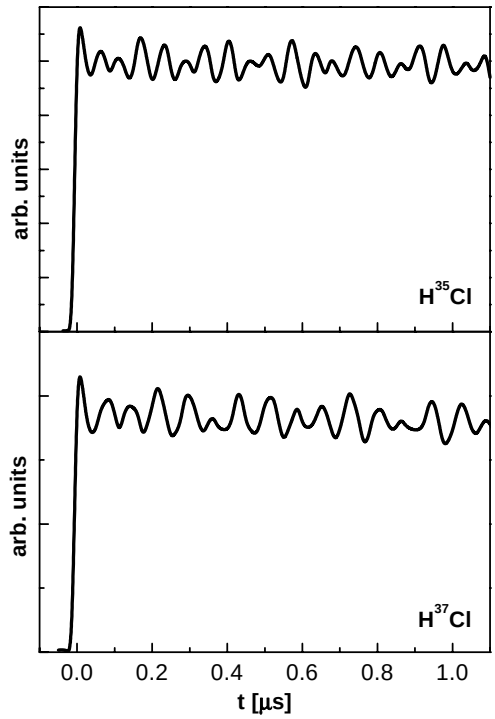

Fig. 6. Time evolutions recorded for the $J = 2$ rotational states of $H^{35}Cl$ and $H^{37}Cl$ exhibiting hyperfine quantum beats. The modulation depth is noticeably less than that for the $J = 1$ data (Fig. 5). The reason for this difference is discussed in reference [21].

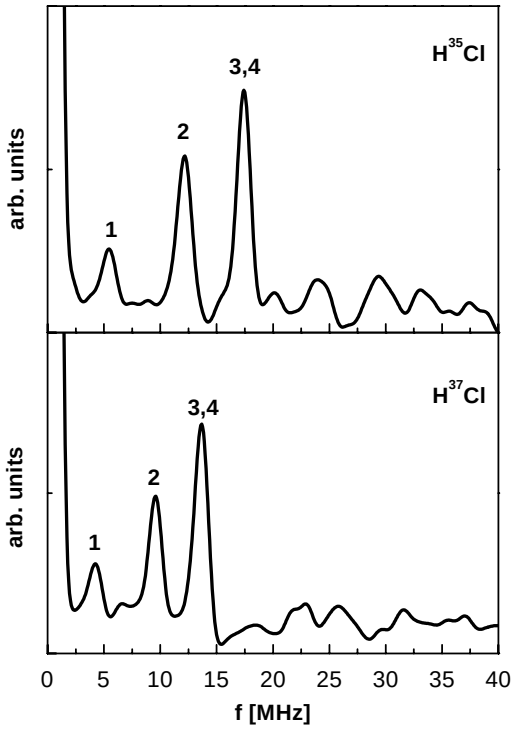

Fig. 8. Frequency domain spectra for the $J = 2$ rotational level in HCl obtained from the real part of the Fourier transform for the time evolutions shown in Figure 6. The labels refer to the coherences detailed in Figure 4.

Table 1. Nuclear hyperfine coupling constants for $H^{35}Cl$ and $H^{37}Cl$.

	$v = 1$, $J = (1, 2)$	$v = 1$, $J = 1$[a]	$v = 1$, $J = 1$[b]
$H^{35}Cl$: eQq [MHz]	−69.51(22)[c]	−69.27289(46)	−69.186(21)
$H^{37}Cl$: eQq [MHz]	−54.40(16)	–	−54.528(17)
$H^{35}Cl$: C_I [MHz]	0.068(10)	0.058597(22)	0.058578(44)
$H^{37}Cl$: C_I [MHz]	0.049(8)	–	($v = 0$) 0.044738(14)

[a]Data from reference [7]. [b]Data from reference [8]. [c]Numbers in parentheses are the standard deviations in the final significant figures.

performed in the following manner. The data with $t \geq 0$ was extracted and extended with zeroes to 1024 points, allowing a smoother form in the FFT (fast Fourier transform) to be obtained. The data was then windowed by a Gaussian function centered at zero with $\tau = 0.4$ μs and the FFT was taken. The parameter τ in the windowing function essentially determines the peak width in the frequency domain; its value was chosen to minimise the linewidth while still suppressing any ringing in the FFT.

The real part of the FFT for both the $H^{35}Cl$ and $H^{37}Cl$ isotopomers are shown in Figures 7 and 8. Inspection of Figure 7 shows that two beats are present in the FFT as can be surmised from the time evolutions given in Figure 5. From Figure 4 however, three hyperfine beats are expected for the $J = 1$ level. We assign the observed quantum beats to the coherences labeled 1 and 2 in Figure 4. This assignment is based on the agreement with predicted frequencies from the vibrational ground state quadrupole parameters [7] and the calculated beat intensities, obtained according to the procedure given in reference [17]. These indicate that beat 3 between $F = 3/2$ and $F = 1/2$ should be considerably weaker than beats 1 and 2. In the case of $J = 2$, Figure 4 indicates that five beats should be observed, of which two (coherences 3 and 4) have the same frequency. In the spectrum of Figure 8 only coherences 1, 2 and 3 are discernible above the noise. In analysing the data we first attempted to fit the quadrupole coupling constants eQq to the measured frequencies. The results were not entirely satisfactory because of a small but significant systematic shift, which was assigned to the nuclear spin-rotation interaction of the ^{35}Cl and ^{37}Cl nuclei. Taking this effect into account, we obtained an excellent fit and determined the value of both eQq and C_I for both the ^{35}Cl and ^{37}Cl isotopomers of HCl in the $v = 1$ vibrational level. We note that in the current configuration, only the relative signs on the parameters were determined from the quantum beat data. The sign of the quadrupole coupling constant was chosen to be the same as that determined previously [8]. The results of this extended least squares fit procedure are summarised in Table 1.

4.2 Pyrimidine

The hyperfine quantum beats in the states $J_{K_a,K_c} = 1_{10}$ and 1_{01} of pyrimidine were prepared in the C–H stretch vibration ν_{13}. This vibration has A_1 symmetry in the molecular point group C_{2v}, leading to a b-type rotational transition located at 3047 cm^{-1} [22]. Detection was carried out *via* the 13^0_1 $S_1 \leftarrow S_0$ transition at 28025 cm^{-1}. Hyperfine quantum beats for the 1_{10} rotational state were investigated using $1_{10} \leftarrow 1_{01}$ pump and $0_{00} \leftarrow 1_{10}$ probe transitions, while for the 1_{01} state the $1_{01} \leftarrow 1_{10}$ and $1_{01} \leftarrow 1_{01}$ transitions were used for pump and probe, respectively. To make sure that the correct pump and probe transitions were selected, the following iterative procedure was adopted. Initially the OPO was used broadband to pump the Q branch of the infrared transition, ensuring that a wide range of rotational levels in the $v_{13} = 1$ level were populated. Then the probe laser was scanned, recording the 13^0_1 $S_1 \leftarrow S_0$ band. In this c-type axis switched transition [23] the R(1) transitions could be easily identified, although the K structure remained unresolved. With the probe laser tuned to the R(1) transitions, the OPO was scanned with the intra-cavity etalon installed to identify all contributing pump transitions. The assignment was obtained in comparison with a simulated double resonance spectrum, calculated with an adopted rotational spectrum simulation for asymmetric top molecules [24]. After the OPO was tuned to the pump transition of interest, the probe laser was scanned to verify the assignment (for example the 1_{10} level shows only an R and P line in the UV check scan) and to identify the correct probe transition. Used in this manner, the double resonance technique allowed a *single* rovibrational state to be unambiguously selected even when the IR and UV lasers could not individually resolve the K structure of the pump and probe transitions.

As pyrimidine also fluoresces when excited to the S_1 state [22], the experiment was performed with both LIF and REMPI detection allowing the suitability of the two techniques for double resonance quantum beat detection to be compared. Pyrimidine has an ionisation potential of 9.23 eV [25]; it was ionised *via* a (1+2) REMPI scheme, which consists of the resonant absorption step to the $^0 0$ S_1 level, followed by a two photon absorption to ionisation (3 photon ionisation at $\lambda \sim 356$ nm). For both LIF and REMPI measurements, a sampling interval of 100 ns was selected, corresponding to a detection bandwidth of 5 MHz, and the time evolution was recorded over an observation time of 6 μs. Figure 9 shows the time evolutions recorded for the 1_{10} state and reveals that the LIF and REMPI results have very similar appearances. The FFT was performed in the same manner as for HCl except that

the Gaussian parameter τ of the window function was chosen to be 3 μs. The real parts of the FFTs recorded for the 1_{10} state with both LIF and REMPI detection are depicted in Figure 10 together with a simulation of the data, carried out as described in Section 3.2. The labels of the quantum beats used in the simulation correspond to the coherences indicated in Figure 4. Eight coherences in total are possible, leading to seven quantum beat frequencies as beats 4 and 5 are degenerate. The extraction of the nuclear hyperfine coupling constants of our data was performed as follows. The beats 2, 4 and 6 from the 1_{10} and 1_{01} measurements were used for the evaluation of χ_{aa} and χ_{cc} while the third diagonal element χ_{bb} was obtained by using the Laplace equation $\sum_i \chi_{ii} = 0$. As discussed above, only the relative signs of the parameters were determined in the analysis. The results of the linear least squares fit are given in Table 2.

Table 2. Nuclear quadrupole coupling constants for pyrimidine.

	$v = 1,\ J = 1$	$v = 1,\ J = 1$[a]	$v = 0$[b]
χ_{aa} [MHz]	$-3.095(9)$[c]	$-3.051(21)$	$-3.107(14)$
χ_{bb} [MHz]	$-0.227(16)$	$-0.289(38)$	$-0.223(16)$
χ_{cc} [MHz]	3.322(13)	3.340(43)	3.330(14)

[a]Data from reference [5]. [b]Data from reference [9]. [c]Numbers in parentheses are the standard deviations in the final significant figures.

5 Discussion

5.1 HCl

Figures 5–8 illustrate the results of our measurements on the $v = 1$ level of $H^{35}Cl$ and $H^{37}Cl$. The time evolutions and their FFTs exhibit quantum beats arising from coherences excited between hyperfine components in a single rotational level. After fitting the appropriate Hamiltonian (Eqs. (2, 3)), we found the hyperfine splittings to be dominated by the electric quadrupole interaction, although the influence of the chlorine nuclear spin-rotation interaction could also be discerned. The respective coupling constants eQq and C_{I} are summarized in Table 1 for both isotopomers. Also given in Table 1 are the results of two previous studies [7,8]. The hyperfine parameters themselves are larger for the ^{35}Cl isotopomer than for the ^{37}Cl species, due to the larger electric quadrupole and magnetic dipole of this nucleus. We note that the ^{37}Cl nucleus possesses a magic number of neutrons (20) and thus has a more spherical shape [26]. Comparison of C_{I} for $H^{37}Cl$ $v = 1$ with the value for $v = 0$ shows an increase with vibrational quantum number as found for the $H^{35}Cl$ isotopomer [8]. Typical errors are on the order of 200 kHz for the quadrupole and 10 kHz for the nuclear spin-rotation parameters respectively. This illustrates both the capability of the quantum beat technique in extracting very high resolution spectroscopic data recorded with relatively broad band lasers and the applicability of the IR-UV double resonance method for making measurements on vibrationally excited levels of the electronic ground state.

Of the previous studies, the recent work by Winnewisser and coworkers [8] provides a comparison to our results. Here pure rotational transitions in HCl were investigated in a static gas sample for both the $v = 0$ and $v = 1$ vibrational levels using direct absorption spectroscopy. The quadrupole coupling constants in $v = 1$ and $v = 0$ as well as the nuclear spin-rotation parameters C_{I}(H) and C_{I}(Cl) for $v = 0$ ($H^{35}Cl$ and $H^{37}Cl$) and $v = 1$ ($H^{35}Cl$) were determined. Their results and our measurements are in agreement to within statistical error. The major difference in the data however is the magnitude of the uncertainties with those of Winnewisser and coworkers being an order of magnitude less than those in the present work. The reason for this lies in the use of saturation techniques in the sub-millimeter wave work, which provides a linewidth of 25 kHz to be achieved. This allowed the splittings of ~ 50 kHz due to the H hyperfine structure to be resolved and C_{I}(H) to be determined.

In the present work, typical full width half maximum (FWHM) in the FFT are ~ 1.2 MHz as determined by the Gauss window used in the analysis and the relatively short observation time for the HCl measurements. This results from the short sample interval of 12.5 ns required to achieve sufficient bandwidth to detect the HCl quantum beats. At present, laser drift limits the number of points in the time evolution that can be recorded, thus restricting the observation time of 1.2 μs in this case. In principle, the anticollinear excitation geometry permits the time evolutions to be measured for much longer periods. For the pyrimidine measurements we were able to record data over 6 μs without loss of signal and we have found that the UV double resonance signal may be detected up to 60 μs after the IR pump pulse. Thus an increase of over an order of magnitude in resolution lies within the capabilities of the technique.

5.2 Pyrimidine

The measurements on pyrimidine provide a direct comparison between the REMPI and LIF methods for ground state quantum beat detection. The REMPI method has the advantage over LIF in that an extended range of molecules can be investigated, including those with zero or low fluorescence yield. It also facilitates a more flexible choice of detection channels in molecules for which only one excited electronic state has a substantial fluorescence yield. The broad applicability of the REMPI technique is illustrated by the two one-colour schemes used in this work: $(2+1)$ for HCl and $(1+2)$ for pyrimidine. On signal intensity grounds we find that there is little difference between the two detection methods. However the necessity of focusing the probe laser for one-colour detection gives rise to substantial power broadening. We find the linewidth in the REMPI double resonance spectra to be approximately twice that in the corresponding LIF spectra. This loss of spectral resolution in the REMPI measurements makes

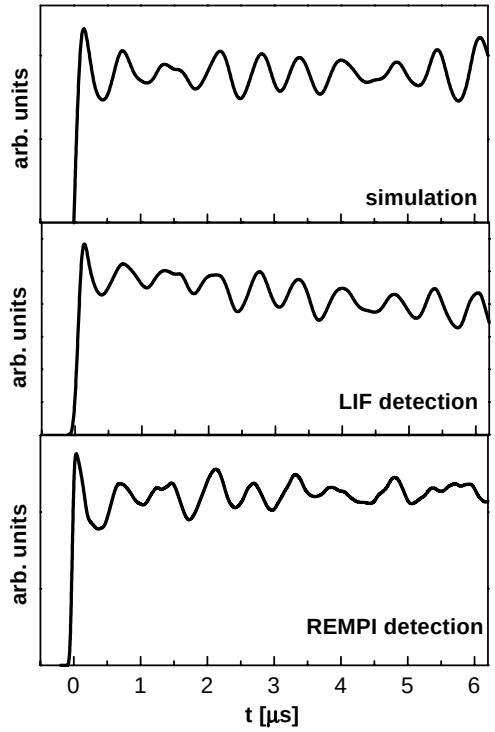

Fig. 9. Time evolutions recorded for the 1_{10} level in pyrimidine using LIF and REMPI detection. A simulation, performed as discussed in the text, is given for comparison.

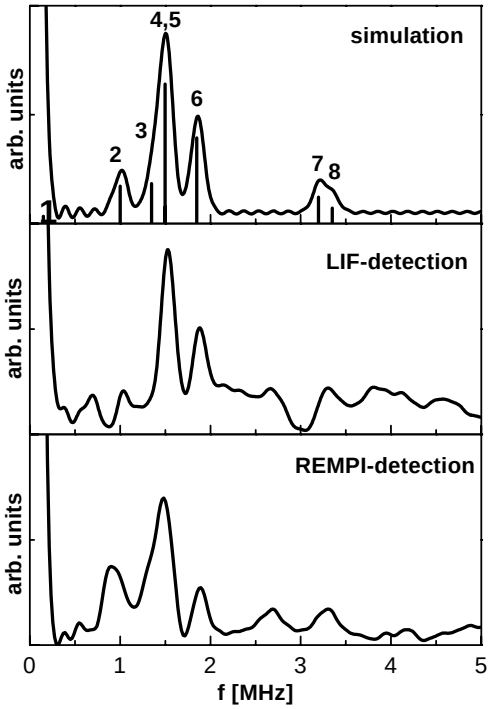

Fig. 10. FFT of the pyrimidine data shown in Figure 9. The labels of the beats refer to the coherences detailed in Figure 4.

the identification of the individual pump and probe transitions more difficult than for the LIF experiments. However this problem could be easily circumvented by using two color $(1 + n')$ REMPI detection.

The quadrupole hyperfine parameters obtained for pyrimidine in the $v_{13} = 1$ level [22] are summarised in Table 2. For comparison the values determined in our previous study [5] are also given. From the data it can be seen that the results of the two studies are in agreement within the statistical error but that the uncertainties in the parameters of our work are ~ 2 times less that those previously. As discussed above this is directly due to the extension of the observation time from ~ 2 μs to ~ 6 μs, owing to the anticollinear excitation geometry. The effect of this decrease in the FFT linewidth is particularly striking when Figure 10 and Figure 1 in reference [5] are compared. We note that the phase of the quantum beats in the two studies are opposite, and that the modulation depth in the present work is 50% that of the previous work. This is a consequence of the perpendicular pump and probe polarisations and makes higher demands on the detection system. The acquisition of a half-wave plate for the OPO will allow us in the future to correct this difficulty. Also given in Table 2 are the quadrupole coupling constants for the vibrational ground state obtained from microwave spectroscopy [9]. The statistical errors in the two sets of parameters are of the same magnitude, demonstrating the suitability of the quantum beat method to such measurements in polyatomic molecules. Furthermore the parameters are the same to within experimental error, confirming the conclusion in our preliminary report [5] that the quadrupole structure of pyrimidine should remain essentially unchanged on excitation of a C–H stretch, as the vibrational mode is spatially isolated from the quadrupolar nuclei.

5.3 Applications of the technique

Comparison with conventional absorption methods shows similar uncertainties in the case of the pyrimidine microwave measurements. For HCl where saturation techniques could be applied, our resolution is somewhat less but we have shown that a substantial increase in the experimental resolution lies within the capabilities of the method. The IR-UV double resonance method has advantages over continuous absorption techniques in that it can easily be applied to a jet-entrained sample and is pulsed in nature. The jet-environment is well suited for preparing many types of unstable species, such as transient radicals, van der Waals molecules and molecular clusters, which are difficult to prepare in a static gas cell. Quantum beat measurements on such species may be used to hyperfine splittings, dipole moments and g-factors yielding high quality data on the molecular geometry and electronic structure in these species. The pulsed nature of the method also lends itself well to the investigation of vibrational overtones. Hyperfine structure in such vibrational levels allows high quality data high up in the potential well to be obtained. In addition to structural parameters discussed above, it is also possible to investigate intra- and (in the case of clusters) intermolecular dynamics using the IR-UV quantum beat method. Such data has been

obtained on excited electronic states using the quantum beat method and has proved to be very useful [2,3].

6 Conclusion

This work presents an extension of the optical quantum beat spectroscopy to the molecular electronic ground state. Using double resonance spectroscopy with an IR pump and a UV probe with LIF and/or REMPI detection, the versatility of the method was demonstrated by measuring the nuclear hyperfine structure in selected rovibrational levels in the electronic ground states of a diatomic (HCl) and a polyatomic (pyrimidine) molecule. The long lifetime of the excited vibrational levels provided a resolution of ~ 150 kHz for HCl and ~ 80 kHz for pyrimidine. The nuclear quadrupole and spin-rotation coupling constants obtained confirm those obtained from conventional absorption techniques, with uncertainties approaching (in the case of HCl) or are comparable with (pyrimidine) those previously determined. Furthermore by improving the frequency stabilisation of the IR laser and increasing the repetition rate, an increase of an order of magnitude in resolution should be possible with this method.

As pulsed narrow-band IR laser sources become available and affordable, selective and coherent excitation of the pertinent normal modes and overtones in a molecule is possible. This allows us for example to study the dependence of the nuclear quadrupole interaction on vibrational mode and hence to gain high quality data on the potential well. High resolution studies on jet-cooled species such as radicals and van der Waals complexes are also made possible with this method. Owing to the long lifetime of vibrationally excited ground state levels, the resolution of the method will ultimately be limited by the window over which the time evolution of the species can be observed. In the present work, this time window is ~ 6 μs but we have shown that an extension to at least 60 μs should be possible. However the full resolution of this Doppler-free time domain method may perhaps only be fully exploited when used in conjunction with a trap for supercool molecules, particularly in regions of the spectrum where convenient narrowband cw lasers are lacking. Such a device has recently attracted much attention [27].

We would like to thank Dr. Herbert Bitto and Prof. Thomas Walther for their assistance in the early stages of this work. Support of this work by the Schweizerischer Nationalfonds zur Förderung der wissenschaftlichen Forschung is gratefully acknowledged.

References

1. E. Hack, J.R. Huber, Int. Rev. Phys. Chem. **10**, 287 (1991).
2. H. Bitto, J.R. Huber, Acc. Chem. Res. **25**, 65 (1992).
3. H. Bitto, J.R. Huber, in *Nonlinear Spectroscopy for Molecular Structure Determination*, edited by R.W. Field, E. Hirota, J.P. Maier, S. Tsuchiya (Blackwell Science, Oxford, 1998).
4. Th. Walther, H. Bitto, J.R. Huber, Chem. Phys. Lett. **209**, 455 (1993).
5. R.T. Carter, Th. Walther, H. Bitto, J.R. Huber, Chem. Phys. Lett. **240**, 79 (1995).
6. A.J. Orr-Ewing, W.R. Simpson, T.P. Rakitzis, R.N. Zare, Isr. J. Chem. **34**, 95 (1994).
7. E.W. Kaiser, J. Chem. Phys. **53**, 1686 (1970).
8. T. Klaus, S.P. Belov, G. Winnewisser, J. Mol. Spectry. **187**, 109 (1998).
9. G.L. Blackman, R.D. Brown, F.R. Burden, J. Mol. Spectry. **35**, 444 (1970).
10. T.K. Minton, S.A. Reid, H.L. Kim, J.D. McDonald, Opt. Commun. **69**, 289 (1989).
11. W.C. Wiley, I.H. McLaren, Rev. Sci. Instrum. **26**, 1150 (1955).
12. H.W. Kroto, *Molecular Rotation Spectra* (Wiley, London, 1975).
13. R.N. Zare, *Angular Momentum* (Wiley, New York, 1988).
14. A.H. Saleck, T. Klaus, S.P. Belov, G. Winnewisser, Z. Naturforsch. A. **51**, 898 (1996).
15. R.J. Myers, W.D. Gwinn, J. Chem. Phys. **20**, 1420 (1952).
16. G.W. Robinson, C.D. Cornwell, J. Chem. Phys. **21**, 1436 (1953).
17. K. Blum, *Density Matrix Theory and Applications* (Plenum Press, New York, 1981).
18. A. Corney, *Atomic and Laser Spectroscopy* (Clarendon Press, Oxford, 1977).
19. A.R.H. Cole, R.N. Jones, R.C. Lord, E.K. Plyler, *Tables of wavenumbers for the calibration of infrared spectrometers* (Pergamon, Oxford, 1977).
20. Y. Xie, P.T.A. Reilly, S. Chilukuri, R.J. Gordon, J. Chem. Phys. **95**, 854 (1991).
21. M. Dubs, J. Mühlbach, H. Bitto, P. Schmidt, J.R. Huber, J. Chem. Phys. **83**, 3755 (1985).
22. K.K. Innes, I.G. Ross, W.R. Moomaw, J. Mol. Spectry. **132**, 492 (1988).
23. J.A. Konings, W.A. Majewski, Y. Matsumoto, D.W. Pratt, W.L. Meerts, J. Chem. Phys. **89**, 1813 (1988).
24. `WANG.FOR`, D. Luckhaus:
e-mail: `dalu@ir.phys.chem.ethz.ch.`
25. *CRC Handbook of Chemistry and Physics*, edited by D.R. Lide (CRC Press, Boca Raton, 1995).
26. T. Mayer-Kuckuk, *Kernphysik: eine Einführung* (Teubner, Stuttgart, 1984).
27. J.D. Weinstein, R. deCarvalho, T. Guillet, B. Friedrich, J.M. Doyle, Nature **395**, 148 (1998).